Int. J. Electrochem. Sci., 9 **(2014)** 5907 - 5923

International Journal of
ELECTROCHEMICAL
SCIENCE
www.electrochemsci.org

Electrodeposition of Hydroxyapatite Coating on AZ91D Alloy for Biodegradable Implant Application

Ivana Škugor Rončević[1,*], *Zoran Grubač*[1], *Mirjana Metikoš-Huković*[2]

[1]Department of General and Inorganic Chemistry, Faculty of Chemistry and Technology, University of Split, N. Tesle 10, 21000 Split, Croatia
[2]Department of Electrochemistry, Faculty of Chemical Engineering and Technology, University of Zagreb, P.O. Box 177, 10000 Zagreb, Croatia
[*]E-mail: skugor@ktf-split.hr

Received: 4 June 2014 / *Accepted:* 27 June 2014 / *Published:* 25 August 2014

The similarity of mechanical properties of Mg and human bones makes Mg and Mg-alloys a potential material for biodegradable implants. However, Mg and Mg alloys corrode too quickly in the tissue fluids, thereby losing mechanical integrity before the tissues have sufficient time to heal. In order to reduce the corrosion rate and enhance the biocompatibility of the Mg-alloy (AZ91D), alloy surface was modified with the hydroxyapatite (HAp) coatings. Hydroxyapatite (HAp) coating on AZ91D alloy substrate was prepared by an electrodeposition method and via chemical deposition by an alternative immersion method (AIM). The as-electrodeposited alloy specimen was post-treated with hot alkali solution to convert the electrodeposited calcium hydrogenphosphate coatings into the bone-like hydroxyapatite coatings. The barrier properties of the HAp coatings were studied using the cyclic voltammetry and electrochemical impedance spectroscopy. The protectiveness of the coatings with different treatment times was investigated by a polarization test in a Hanks' solution. The results revealed that hydroxyapatite coating significantly reduced the localized corrosion of the alloy, which is critical for better in-service mechanical integrity. Fourier transform infrared spectroscopy (FTIR) was used to verify the existence of the HAp coating and its morphology on AZ91D alloy surface.

Keywords: Magnesium alloy, biocompatibility, hydroxyapatite, electrodeposition, surface modification

1. INTRODUCTION

Stainless steels, cobalt-based alloys and titanium alloys are widely studied and applied clinically in hard tissue implants, especially in load-bearing applications, due to their high strength, ductility and good corrosion resistance [1]. These orthopedic implants provide mechanical support during the initial period of bone healing. When bone fracture healing is completed, the presence of the

implant could be a nuisance because it may cause stress shielding to the neighboring bone structure, leading to osteoporosis [2]. Long-term adverse effects or even an increased risk of local inflammation may occur after long-term implantation since the metallic implant is a foreign body to human tissues [3]. For young patients, permanent bone plates would also restrict bone growth. In view of these adverse effects, removal of the bone plates by a second surgery is generally recommended after bone healing has completed. However, removal of bone plates by a second surgery means risk, stress, and economic burden to the patient [2]. To reduce such complications, the use of biodegradable metallic implants has been investigated [3]. Biodegradable implant materials in the human body can be gradually dissolved, absorbed, consumed or excreted, so there is no need for the secondary surgery to remove implants after the surgery regions have healed [4]. Currently, degradable implants are made of polymer materials. Owing to the low mechanical strength, polymeric implants are used only in low load-bearing applications [5]. Thus the development of high load-bearing degradable orthopedic implants is an attractive idea for bone fracture healing. Magnesium (Mg), by virtue of its desirable mechanical properties, non-toxicity, and degradability, is a potential candidate metallic material for degradable implants [6]. According to a recent review by Staiger et. al, [6] the mechanical properties of Mg are close to those of bones, and Mg is non-toxic and excess of Mg in human body can be easily excreted via urine. Magnesium possesses good biocompatibility and relatively large amounts of magnesium are tolerated by the body without ill effect [7]. A fully biocompatibile biomaterial should elicit a minimal inflammatory response, together with the desired specific tissue response [8]. Dissolved Mg ions may promote bone cell attachment, tissue growth at the implants, and can be applied in surgical as well as in cardiovascular treatments [9]. Magnesium alloys possess a density of ~ 1.7–2.0 g cm^{-3} that is close to that of natural bones (1.8–2.1 g cm^{-3}) and the compressive strength and tensile strength are much higher than those of biodegradable polymers. Compared with Ti alloys (110–117 GPa), stainless steels (189–205 GPa), and Co–Cr alloys (230 GPa), the elastic modulus of magnesium alloys (41–45 GPa) is closer to that of natural bones. Hence, the stress shielding effect induced by serious mismatch in the elastic module between natural bones and implants can be mitigated [10]. Also, compared with poly-96L/4D-lactide, the magnesium alloys AZ31 and AZ91 enhanced the ontogenesis response and increased the newly formed bone [11]. Degradable metal implants made of magnesium alloys were introduced into orthopedic and trauma surgery in the first half of the last century [12]. However, pure magnesium and its alloys possess poor corrosion resistance and degrade too fast at physiological pH 7.4-7.2 as well as in physiological media containing high concentration of aggressive ions (chloride ions (~104 mmol L^{-1}) [10]), thereby losing mechanical integrity before tissues have sufficient time to heal (over a timescale of 12-18 weeks while the bone tissue being replaced by natural tissue [13]) [14]. Magnesium and its alloys are generally known to degrade in aqueous environments via an electrochemical reaction (corrosion) which produces magnesium hydroxide and hydrogen gas [15]. The aggressive behavior of chloride ions to Mg alloys has been widely investigated and it is generally accepted that chloride ions can transform the protective $MgO/Mg(OH)_2$ into soluble $MgCl_2$ thus accelerating magnesium dissolution [1,10,15]. In magnesium and its alloys, elements (impurities) and cathodic sites with low hydrogen overpotential facilitate hydrogen evolution, thus causing substantial galvanic corrosion rates [15]. The very low corrosion resistance of magnesium alloys caused the failure of the first studies on the application of magnesium

alloys for orthopedic implant devices. A hydrogen gas cavity was formed around the implant devices accompanying the corrosion of the alloy [16,17,18]. This cavity will delay healing of the surgery region and lead to necrosis of tissues, because they can cause separation of tissues and tissue layers. Up hydrogen evolution local alkalization will be inevitable around a rapidly corroding magnesium implant. The local alkalization can unfavorably affect the pH dependent physiological reaction balances in the vicinity of the magnesium implant and may even lead to an alkaline poisoning effect if the local in vivo pH value exceeds 7.8 in that region [4]. Because of that the degradation products, such as Mg^{2+}, H_2 and OH^-, should be within the body's acceptable absorption levels [13], according to Zeng et al., 0.01 ml cm^{-2} H_2 per day is a tolerated level in the human body [9]. This revealed the importance of controlling the corrosion rate of the alloy in the human body [18]. The enhancement of the corrosion resistance of magnesium and improvement of the lifetime of Mg alloys can be achieved by using different modification methods such as alloying, different chemical treatments and various surface treatments such as deposition of chemical conversion layers, [19] treatments based on the sol–gel application [20], and the surface modification by formation of SAMs [2,21,22]. Furthermore, the surface biocompatibility of Mg can also be enhanced using bioactive coatings, such as calcium phosphate coatings [23,24,25]. Among them, hydroxyapatite (HA) coatings are well recognized because of their excellent bioactivity, which improves the bonding between the metal implant and the bone [26]. But the mechanical strength of HA is too poor to be used in load-bearing applications. Therefore, HA coating was deposited on the surface of metallic implants to improve the biocompatibility property [27]. So far, HA coating on Ti alloy substrate used as implanted materials has been deeply studied [28,29]. However, the deposition of HA coating on Mg alloy substrate and the corresponding degradation behavior in simulated body fluid (SBF) are rarely investigated. Many methods such as plasma spraying, pulse laser melting, and physical vapor deposition cannot be used to deposit HA coating on Mg alloy because of its low melting point and poor heat resistance. Electrochemical deposition has unique advantages due to its capability of forming uniform coating and simple setup. In addition, the deposition processing can be conducted at room temperature and the morphology of coating can be controlled easily by varying the electrochemical potential and other parameters [23,29].

In this paper we report the preparation of hydroxyapatite (HAp) coatings on magnesium AZ91D alloy by electrodeposition and subsequent treatment in alkaline (NaOH) solution and by an alternative immersion method (AIM). The barrier properties of the coatings in the Hanks' solution were investigated using electrochemical impedance spectroscopy (EIS) and voltammetry methods. Morphology of the HAp coatings was studied using Fourier transform infrared spectroscopy (FTIR).

2. EXPERIMENTAL

Working electrodes were the chips of AZ91D alloy with the wt% content of: 8.6 Al, 0.51 Zn, 0.19 Mn, 0.05 Si, 0.025 Cu, 0.004 Fe and balance Mg. The cylinder shaped working electrodes, having a surface area of 0.235 cm^2, were sealed into glass tubes with Polirepar S. Before HAp deposition the electrodes were abraded with fine emery paper, polished with alumina powder down to 0.05 μm,

degreased in ethanol in an ultrasonic bath, rinsed with distilled water, kept immersed in 1.0 M solution of NaOH at 80 ^{o}C for 1 h, and rinsed with distilled water. Electrodeposition of HAp was carried out at constant potential values of −2.0 V for different periods of time in a solution (100 cm^3) containing 50 cm^3 0.1 mol dm^{-3} $Ca(NO_3)_2$ and 0.06 mol dm^{-3} $NH_4H_2PO_4$. The pH value of solution was 5 (adjusted with 0.5 mol dm^{-3} HNO_3). During deposition the solution was stirred with a magnetic stirrer. After deposition, the electrodes were immersed in 1.0 mol dm^{-3} solution of NaOH at 80 ^{o}C for 1 h, rinsed with distilled water and air-dried. The corrosion resistance of HAp deposit modified specimens was investigated at 37 ^{o}C in a Hanks' solution, pH 6.67, of the following composition (g dm^{-3}): NaCl 8.00, KCl 0.40, $NaHCO_3$ 0.35, $NaH_2PO_4 \times \cdot H_2O$ 0.25, $Na_2HPO_4 \times \cdot 2H_2O$ 0.06, $CaCl_2 \times \cdot 2H_2O$ 0.19, $MgCl_2$ 0.19, $MgSO_4 \times \cdot 7H_2O$ 0.06, and glucose 1.00. All chemicals were of p.a. purity. All electrochemical experiments were carried out in a standard three-electrode cell containing 100 cm^3 of Hanks' solution. The counter electrode was a large area platinum electrode and the reference electrode, to which all potentials are referred, was an Ag/AgCl/3 M KCl (209 mV vs. SHE). Before measurements the electrodes were stabilized for 0.5 h in a Hanks' solution. Potentiodynamic measurements were performed at a sweep rate of 10 mV s^{-1}. EIS measurements were performed at the open circuit potential (E_{OCP}) in the frequency range from 100 kHz to 0.1 Hz with an *ac* signal ±5 mV. Measurements were carried out using a Solartron Frequency Response Analyzer SI 1255 and Solartron Electrochemical Interface 1287 controlled by a PC. Impedance data were fitted by a suitable electrical equivalent circuit (EEC) model, employing the complex non-linear least squares (CNLS) fit analysis [30] offered by the Solartron ZView® software. The fitting quality was evaluated by the chi-squared and relative error values, which were in the order of 10^{-3}-10^{-4} and below 5 %, respectively, indicating that the agreement between the proposed EEC model and the experimental data was good. The HAp deposit was characterized by FTIR. The FTIR spectra were recorded in the 4000–650 cm^{-1} region with the scan resolution of 4 cm^{-1} using Horizontal Attenuated Total Reflectance (HATR) method on a Perkin-Elmer Spectrum One FTIR spectrometer.

3. RESULTS AND DISCUSSION

3.1. Electrochemical deposition of hydroxyapatite

Modification of the electrodes with hydroxyapatite film was performed by electrodeposition in a solution (100 cm^3) containing 50 mL 0.1 mol dm^{-3} $Ca(NO_3)_2$ and 50 ml 0.06 mol dm^{-3} $NH_4H_2PO_4$, pH 5 (adjusted with 0.5 mol dm^{-3} HNO_3) at constant potential value of −2.0 V at room temperature. The electrodeposition time was from 30 to 180 min [31]. Reactions on the surface of AZ91D alloy during electrodeposition are:

Step I: reduction of the hydrogen from $H_2PO_4^-$ and HPO_4^{2-}:

$$2\ H_2PO_4^- + 2\ e^- \rightarrow 2\ HPO_4^{2-} + H_2\ (g) \quad (1)$$

$$2\ HPO_4^{2-} + 2\ e^- \rightarrow 2PO_4^{3-} + H_2\ (g) \quad (2)$$

Step II: Ca^{2+} ion reacts with HPO_4^{2-} and PO_4^{3-} and form $CaHPO_4 \times 2H_2O$ (brushite, calcium hydrogenphosphate dihydrate) and $Ca_3(PO_4)_2$ (calcium phosphate, β - TCP):

$Ca^{2+} + HPO_4^{2-} + 2\ H_2O \rightarrow CaHPO_4 \times 2\ H_2O$ (s) (3)

$3\ Ca^{2+} + PO_4^{3-} \rightarrow Ca_3(PO_4)_2$ (s) (4)

Brushite and β - TCP are the precursors to the more stable phase hydroxyapatite, $Ca_{10}(PO_4)_6(OH)_2$, HAp. Alkaline treatment (acid-base reaction) converts brushite and β - TCP film formed on the AZ91D alloy surface by electrodeposition into hydroxyapatite, HAp [32].

$10\ CaHPO_4 \times 2\ H_2O$ (s) + $12\ OH^- \leftrightarrows Ca_{10}(PO_4)_6(OH)_2$ (s) + $4\ PO_4^{3-}$ + $30\ H_2O$ (5)

Kannan [33] and Song [27] were analysed the coating structures of the electrodeposited coatings prior to and after alkaline treatment using X-ray diffraction technique. Their results clearly show that electrodeposited coating prior to alkaline treatment is mainly consisted of calcium phosphate dihydrate and β-TCP. Alkaline treatment results in the Hap coating formation.

Specifically in environments with a pH greater than 6–7, brushite (calcium phosphate dihydrate, $CaHPO_4 \times 2H_2O$) becomes unstable and transforms into the more favourable Hap phase. In the alkaline solutions HAp is the most stable ceramic layer of calcium phosphate. Prior investigations have also utilized the increased solubility of brushite on metallic implants as a means of increasing the amounts of calcium and phosphate ions available in the immediate vicinity of the implant to promote increased osseointegration [34,35]. Acid-base reaction involves the electrode immersion for 1 h in 1 mol dm^{-3} NaOH at 80° C [27,33].

3.2. Barrier properties of the coating

3.2.1. Electrochemical impedance spectroscopy

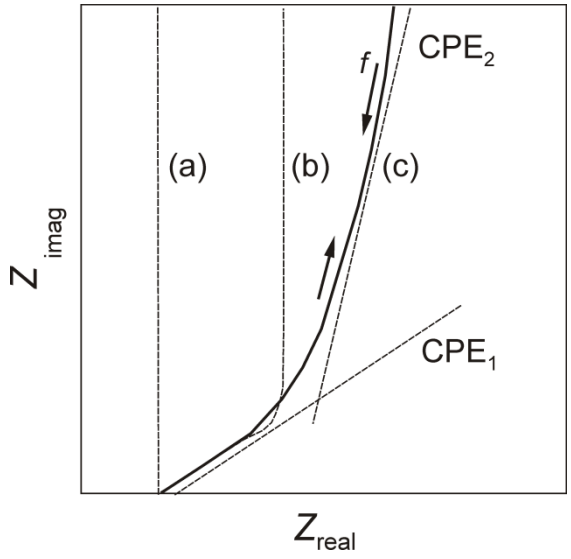

Figure 1. Nyquist plot for various frequency dispersions (a) for an ideally capacitive behavior of plain electrodes; (b) for the in-a-pore dispersion simulated by de Levie's Eq.(9) [41]; (c) for the in-a-pore dispersion and by pore size distribution simulated by TLM-PSD [42].

The impedance of most electrodes deviates from the purely capacitive behavior which is represented as a vertical line in the Nyquist plot, curve (a) in Figure 1. The non-ideality due to

frequency dispersions has been widely described by the constant phase element (*CPE*) that is an empirical distributed element. Its impedance is equal to $Z_{CPE} = [Q\ (j\omega)^n]^{-1}$ [36], where Q is the frequency independent parameter, ω is the angular frequency, and n is the *CPE* power. When n = 1, Q represents the pure capacitance, while for $n \neq 1$ the system shows behaviour that has been attributed to the surface heterogeneity [37], or to the continuously distributed time constants for charge transfer reactions [38].

Frequency dispersion leads to an inclined line whose phase angle is equal to $(\pi / 2)$ n. In Figure 1, curve (b) can be described with the CPE_1 at high frequencies and with an ideal capacitance at low frequencies while curve (c) can be approximated with the CPE_1 at high frequencies and roughly with the CPE_2 at low frequencies [39,40].

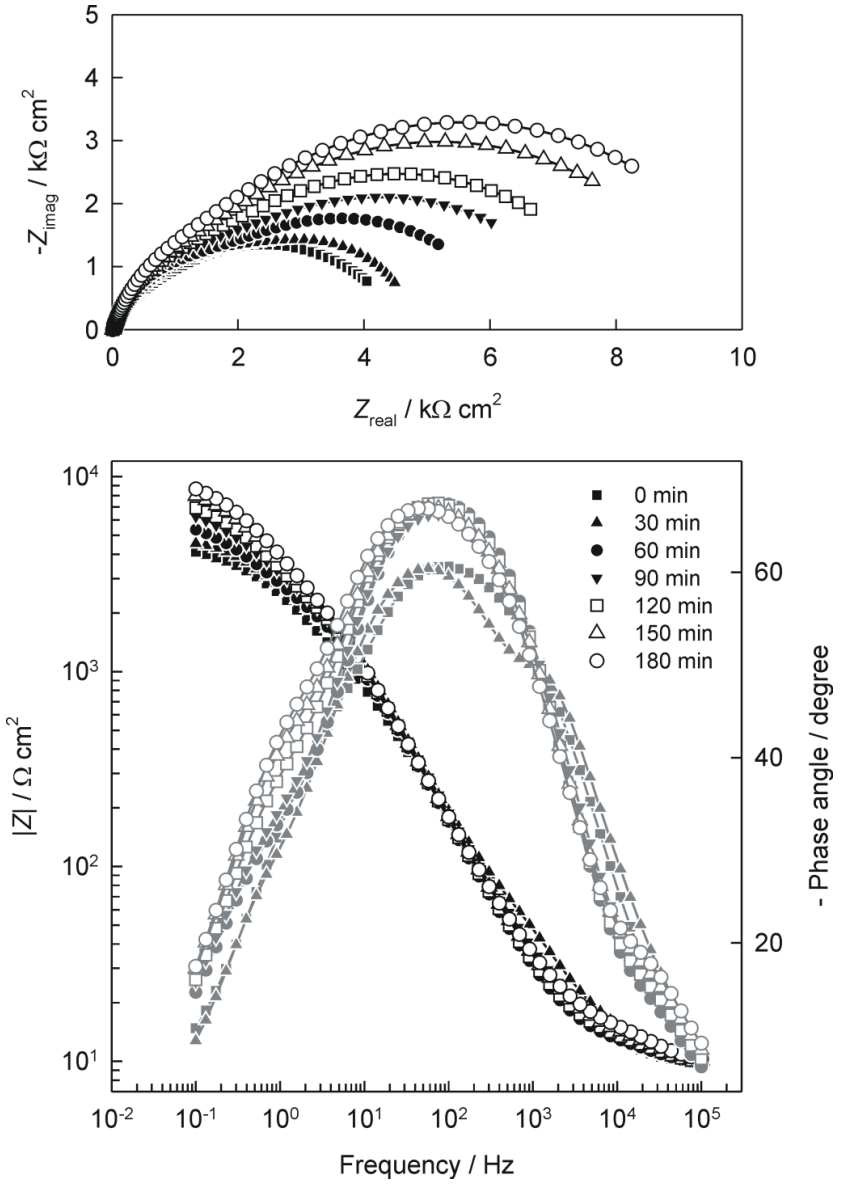

Figure 2. Nyquist and Bode plots for the impedance data recorded with uncoated AZ91D alloy (with a native surface layer) and HAp coated AZ91D alloy in the Hanks' solution (37 ^{o}C) at E_{OCP}. Electrodeposition was performed at −2.0 V for denoted time periods.

In the case of highly porous electrodes, geometric factors are the most important among the origins of frequency dispersion in the absence of faradaic reactions. The non-ideality due to the geometric factors can be divided into two classes; dispersions in a pore and by pore size distribution (PSD) [39,40]. In-a-pore dispersion occurs since the penetration depth, λ of an *ac* signal into a pore decreases with frequency ($f_1 < f_2$; $\lambda_1 > \lambda_2$). Frequency dispersions caused by pore size distribution (PSD) occur due to the presence of pores of various sizes which have different penetration depths even at the same frequency ($r_1 < r_2$; $\lambda_1 < \lambda_2$). Therefore, an apparent capacitance or equivalent series resistance changes with frequency even in the porous materials composed entirely of pores with equal dimension. The in-a-pore dispersion has been modeled by many researchers [42,43] since de Levie [41] simulated it by the transmission line equivalent circuit [44].

Corrosion resistance of AZ91D alloy unmodified and modified with a hydroxyapatite (HAp) film in the Hanks' solution was investigated by EIS. Figure 2 shows the Nyquist and Bode plots of impedance spectra of unmodified and with HAp film modified AZ91D alloy recorded in Hanks' solution at open circuit potential after 30 min of stabilization. The Nyquist plot for unmodified AZ91D alloy show flattened capacitive semicircle with the canter below the real axis.

As compared to the unmodified AZ91D alloy, Nyquist plot for AZ91D alloy modified with hydroxyapatite show higher capacitive semicircle and greater overall impedance. It is also evident that the capacitive semicircle increases with an increase of the electrodeposition time. In the low frequencies region of the Bode plot, it can be seen that the presence of the hydroxyapatite increases the value of log |*Z*| at which dominates the polarization resistance. EIS data recorded for the unmodified AZ91D alloy in Hanks' solution was modelled by the electrical equivalent circuit (EEC) with two time constants shown in Table 1. In the EEC, constant phase element CPE_1 attributed to the double layer capacitance, and R_1 to the charge transfer resistance and CPE_2 and R_2 attributed to the resistance of the film and capacitance of the ions travel through the film. In the case of electrodes modified with hydroxyapatite at low frequency region of the impedance spectra an additional time constant appears. It is attributed to the diffusion processes and described by the Warburg diffusion element W_s.

Therefore, EIS results obtained for AZ91D alloy modified with hydroxyapatite were modelled with the equivalent electrical circuit shown in Table 1, which contains values of the EEK elements. The total impedance, *Z* of the investigated electrochemical system is the sum of the ohmic resistance and the impedance of the electrochemical interface ($Z_{el} + Z_{HF} + Z_{LF}$) and is described by the transfer function:

$$Z(j\omega) = R_{el} + \left\{ Q_1(j\omega)^{n_1} + \left\{ R_1 + \left[Q_2(j\omega)^{n_2} + (R_2 + Z_W)^{-1} \right]^{-1} \right\}^{-1} \right\}^{-1} \quad (6)$$

The polarization resistance represents the sum of R_1, R_2 and a diffusional resistance (R_{S-R}) [45]. The experimental results show that the electrodeposition of hydroxyapatite significantly affects the corrosion behaviour i.e. polarization resistance of the AZ91D alloy in Hanks' solution. The value of polarization resistance increases with an increase of the electrodeposition time. Increases of the electrodeposition time decrease the value of the electrochemical double layer capacitance. Decrease indicates an increase in thickness of hydroxyapatite film as well as the structural changes within the film and the formation of compact HAp film. The microstructure of the inner dense layer is one of the

most important factors of the hydroxyapatite protection. The compact structure is a barrier that protects penetration of electrolyte to the substrate [46]. The increase of polarization resistance values indicates better corrosion protection in Hanks' solution of HAp film electrodeposited over a longer period of time.

In general, the complex plane spectra show a high frequency straight line at 45°, followed by a semicircle in the low frequency region. This behavior is characteristic of porous electrodes, and can be analyzed by a finite length pore model [41,47,48]. Therefore, the EEC includes also the so-called "O" circuit element ("porous bounded Warburg"). The term "O" represents a dimensional diffusion through a layer of finite thickness or the (penetrability) penetration depth of the *ac* signal across pores of finite length.

Table 1. The impedance parameters of uncoated AZ91D alloy and AZ91D alloy samples coated with HAp coatings, obtained in Hanks' solution (37 °C) at E_{OCP}. Electrodeposition was performed at −2.0 V for denoted time periods.

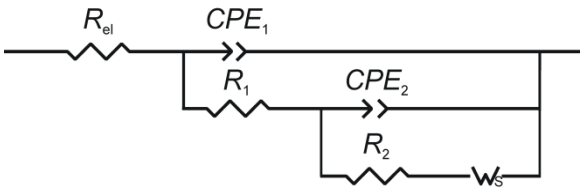

Method	*t* / min	$10^5 \times Q_1$ / Ω^{-1} cm^{-2} s^n	n_1	R_1 / kΩ cm^2	$10^5 \times Q_2$ / Ω^{-1} cm^{-2} s^n	n_2	R_2 / kΩ cm^2	$W_{S\text{-}R}$ / Ω cm^2	$10^3 \times B$ / s$^{0.5}$	$10^3 \times Y_o$ / Ω^{-1} s$^{0.5}$	R_d / Ω cm^2	α_0
ED	-	8.0	0.94	0.2	7.9	0.69	4.4	-	-	-	-	-
	30	4.1	0.77	2.5	20.8	0.91	2.3	18.9	20.0	1.0	19.0	35.3
	60	3.7	0.86	1.5	12.9	0.75	4.9	2.2	3.9	1.7	2.3	183.2
	90	3.7	0.89	1.3	10.3	0.71	6.4	2.4	3.4	1.4	2.5	208.6
	120	4.3	0.88	1.2	8.7	0.75	7.1	2.7	3.9	1.4	2.7	181.3
	150	4.6	0.92	0.8	7.0	0.74	8.9	3.1	3.9	1.3	3.1	180.4
	180	5.1	0.96	0.7	6.2	0.74	9.9	3.7	4.1	1.1	3.7	172.5
AIM		0.6	0.77	0.6	6.4	0.70	9.1	3.6	3.9	1.1	3.5	181.8

R_{el} = 10 Ω cm^2; ED - electrodeposition; AIM - alternative immersion method

The complex impedance $Z_O(\omega)$ is given by the expression:

$$Z_O(\omega) = \frac{1}{Y_O}\frac{\tanh\left[B\sqrt{j\omega}\right]}{\sqrt{j\omega}} \qquad (7)$$

The "O" element is characterized by two parameters, an "admittance" parameter, Y_O, and a "time constant", B (with unit s$^{1/2}$) from which geometric parameters can be examined:

$$Y_O^{-1} = \frac{\sqrt{2}\alpha_0 l_p}{\pi N \kappa r^2}, \qquad Y_O = \frac{\sqrt{W_{S-T}}}{W_{S-R}} \quad B = \sqrt{W_{S-T}} \qquad B^{-1} = \alpha_0\sqrt{2}, \qquad \frac{B}{Y_O} = R_d \quad (8)$$

R_d is the diffusion resistance (i.e. $Z_O(\omega)$ when $\omega \to 0$), κ is the electrolyte conductivity, r is the pore radius, l_p is the pore length, N is number of pores, and α_0 is the penetrability coefficient. The penetrability (α) is the ratio of *ac* signal penetration depth (λ) to the pore length, and is defined as [37]:

$$\alpha = \frac{\lambda}{l_p} \text{ i } \lambda = \left(\frac{1}{2l_p}\sqrt{\frac{\kappa r}{C_{dl}}}\right)\omega^{-0.5} = a_0\omega^{-0.5} \quad (9)$$

C_{dl} is the electric double layer capacitance at the electrode / electrolyte interface, ω is the angular frequency. The numerical value α_0 is directly proportional to $\frac{\sqrt{r}}{l_p}$.

The numerical values of the impedance parameters B, Y_O, R_d, and α, obtained by fitting experimental data, are listed in Table 1. The numerical values for α_0, are significantly higher than 1, which means that $\lambda >> l_p$, i.e., the *ac* signal penetrates to the bottom of the pore and the electrode behaves as a flat one [49].

Curve (b) in Figure 1 shows some common trends of the in-a-pore dispersion models [40] at high frequencies and low penetrability giving the phase angle, $\theta = -\pi / 4$. As penetrability increases (or frequency decreases), the impedance approaches the ideal capacitive behaviour and is shifted along the abscissa by in-a-pore dispersion part. Deviation from ideality even at low frequency, however, has also been observed on many porous materials as shown by curve (c) on Figure 1.

K. H. Lee et. al. [37] suggested the possibility of frequency dispersions due to the pore size distribution (PSD) because the non-ideality cannot be simulated or fitted successfully with the models considering only in-a-pore dispersion. The penetration depth of the *ac* signal becomes distributed even at an identical frequency since the size of each pore determines its own penetration depth. A new model, called the transmission line model with pore size distribution (TLM-PSD) has been developed for reflective boundary conditions, without faradaic reactions, considering the by-PSD dispersion as well as the in-a pore dispersion. The curve (c) in Figure 1 was simulated (was fitted) with the de Levie's and Lee's TLM-PDS models [37, 40].

3.2.2. Polarization measurements

Polarization curves recorded with uncoated and HAp coated alloy specimens, using a scan rate of 10 mV s^{-1}, are shown in Figure 3. The cathodic branch of the polarization curve for all specimens exhibits a linear Tafel region with slope values ranging from −235 mV dec^{-1} to −140 mV dec^{-1}. These numerical values indicate the same mechanism of the hydrogen evolution reaction, which occurs at electrodes covered with a surface film [50]. The values obtained agree well with those reported for Mg-alloys that were unmodified and modified with SAMs of fatty acids or phosphonate SAMs, and immersed in near neutral aqueous solutions containing chloride ions [51,52]. In the anodic region the simultaneous combination of both anodic dissolution and hydrogen evolution (negative different effect) and the localized corrosion have been reported as the main reasons for the complicated anodic polarization behaviour of unprotected Mg alloy [53]. HAp film makes the anodic polarization curves more stable significantly decreasing the anodic current densities. The barrier properties of HAp film depend on the electrodeposition time; the longer the electrodeposition time is, the lower are the values of the cathodic and anodic current density. However, after slow increase of the current density at higher anodic potentials a sharp increase in anodic currents was observed for all specimens indicating the breakdown of the partially protective surface layer [45] which is characteristic for a localized

corrosion. The breakdown potential is dependent on the electrodeposition time: it is shifted towards more positive values extending the deposition time.

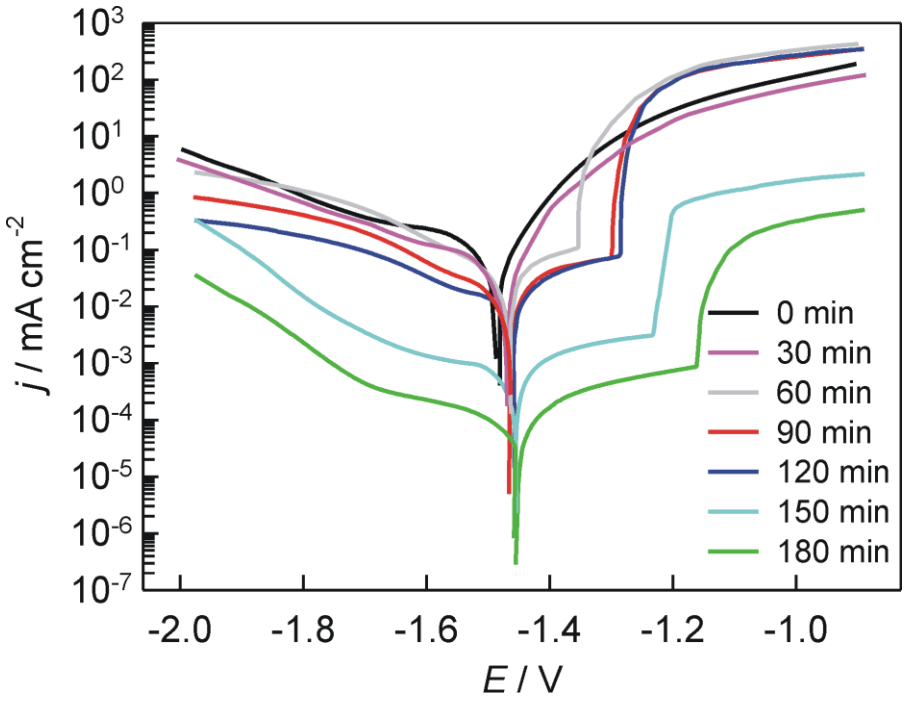

Figure 3. Tafel plots recorded with uncoated AZ91D alloy (with a native surface layer) and HAp coated AZ91D alloy in the Hanks' solution at 37 ^{o}C; v = 10 mV s^{-1}. Electrodeposition was performed at −2.0 V for denoted time periods.

The cathodic and anodic portions of the polarization curves around E_{corr} indicate that the cathodic process is rate determining for a corrosion process of all specimens. Extrapolation of the linear part of the cathodic currents to the corrosion potential was use for a rough estimation of the corrosion current densities (j_{corr}). The numerical values of the corrosion kinetic parameters b_c, b_a, j_{corr} and E_{corr}, obtained by fitting experimental data, are listed in Table 2. The numerical values of the corrosion current densities determined for untreated alloy specimens is 41.2 μA cm^{-2} and for coating HAp films formed on AZ91D alloy for 180 min at −2 V is 0.1 μA cm^{-2}.

Coverage θ of the AZ91D surface by film of hydroxyapatite shown in Table 2 are calculated according to the expression:

$$\theta = (j_{AZ91D} - j_{AZ91D|HAp}) / j_{AZ91D} \quad (10)$$

j_{AZ91D} and $j_{AZ91D|HAp}$ being the corrosion current density values of AZ91D alloy coated with spontaneously formed oxide film (unmodified), or HAp film, respectively. The coverage of HAp coatings ranges from 38 % (electrodeposition time of 30 min) to 99 % (electrodeposition time of 180 min). This indicates that the coating protectiveness against the active dissolution of the substrate is not sufficient when the treatment time is short. With an increase in the treatment time, the coating protectiveness against the active dissolution of the substrate increases. This increase of the protectiveness is due to the enhancement of the barrier effect of the inner layer against the solution

penetration. These results indicate that the corrosion rate of the magnesium can be varied with the microstructure of the HAp coating [54]. The CaP coating protectiveness reported for the systems Mg-alloy/CaP coating/physiological solution range from 60% to 90%, depending on the electrodeposition conditions [27,55].

Table 2. The corrosion kinetic parameters for uncoated AZ91D alloy (0 min) and HAp coated AZ91D alloy in the Hanks' solution at 37 ^{o}C; v = 10 mV s^{-1}. Electrodeposition was performed at −2.0 V for denoted time periods.

t / min	$-b_c$ / mV dec^{-1}	b_a / mV dec^{-1}	j_{corr} / μA cm^{-2}	$-E_{corr}$ / V	θ / %
-	228	139	41.2	1.49	-
30	227	115	25.5	1.48	38
60	177	67	20.8	1.47	50
90	207	41	16.9	1.47	59
120	235	35	16.0	1.46	61
150	184	29	1.1	1.46	97
180	154	21	0.1	1.46	99

3.3. Characterization of HAp coating

3.3.1. Fourier transform infrared spectroscopy

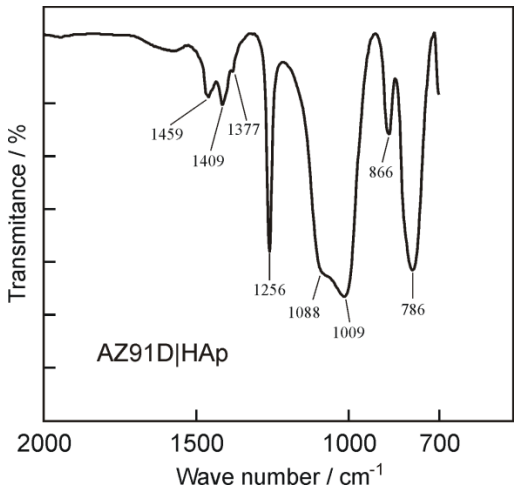

Figure 4. The FTIR spectra of AZ91D alloy coated with electrodeposited HAp coating. Electrodeposition was performed at −2.0 V for 3 h.

Figure 4 shows a FTIR spectrum of AZ91D alloy substrate coated by electrodeposited HAp film that was subsequently alkali treated. A strong ν_3 PO_4^{3-} vibration band, associated with the internal modes of PO_4^{3-} (P-O asymmetric stretching vibrations), are observed inside the frequency range from ca. 1000 cm^{-1} to 1100 cm^{-1} at 1009 cm^{-1} and 1088 cm^{-1} [56-58]. The ν_3 asymmetric P-O stretching

mode is triply degenerate in the free phosphate ion, but this mode is resolved into at least two distinct peaks in crystalline hydroxyapatite [59]. It has been shown that as the crystallinity of the hydroxyapatite increases these two ν_3 bands become increasingly resolved [59]. In our infrared spectrum, the two ν_3 bands are fine- resolved, which indicates that the coating is crystalline [59,60].

The peaks at 1459, 1409 and 1337 cm^{-1} are due to the presence of carbonate ions in the hydroxyapatite structure [61-64]. It is well known that carbonate, generated from reaction of atmospheric CO_2 with aqueous solutions, readily substitutes for phosphate ions (B-type incorporation; i.e., CO_3^{2-} for PO_4^{3-} substitutions [65]) in the crystal structure of hydroxyapatite. The introduction of these different ions was beneficial to the biocompatibility because of natural bone tissue also contained Mg^{2+}, Na^{+}, HPO_4^{2-} and CO_3^{2-} which gives an additional advantage because it leads to an enhanced osseointegration [66,67].

The characteristic peak at around 866 cm^{-1}, has been mostly attributed to carbonate group [62-64,67−69]. However, this peak also indicates the presence of HPO_4^{2-} groups in the coating structure [45,63,69].

This peak could also indicate that there are still remained a small amount of $CaHPO_4 \times 2H_2O$, DCPD due to incomplete conversion to HA by alkali treatment [23]. The FTIR results confirm the presence of HAp film on the AZ91D alloy surface [70].

3.4. Chemical deposition of hydroxyapatite

When it comes to light metals, such as Al and Mg, that have surfaces with mesoporous morphology, the alternative immersion method (AIM) can be used to efficiently deposit synthetic HAp [71]. AIM method is a strikingly simple method to apply Hap coatings to a surface schematically outlined in Figure 5. In the present approach, the specimens were exposed to 20 cycles of alternating immersion in saturated $Ca(OH)_2$ and 0.02 M $NH_4H_2PO_4$. The holding time in each solution was 1 min at room temperature. Between each soaking step and after each cycle, the samples were rinsed in ultrapure water for 1 min. Finally, the samples were dried by nitrogen gas [71].

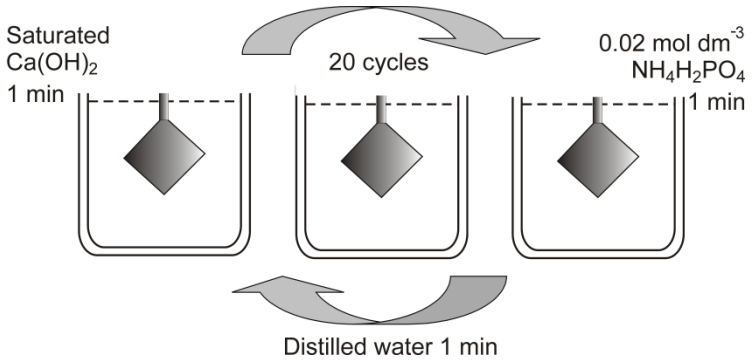

Figure 5. Schematic outline of the AIM treatment leading to chemical deposition of Hap coating [75].

After coating with HAp by AIM barrier properties of coating on the AZ91D alloy surface were investigated by EIS. As the shape of spectra is identical to those presented in Figure 2 it was fitted with the same EEC. The numerical data obtained for impedance parameters are listed in Table 1. From the value of the element Q_2 (table 1) it could be concluded that the hydroxyapatite layer formed by electrodeposition (at −2.0 V for 180 min) is thicker and less porous. Figure 6 shows the values of R_p (very structure-sensitive property) as a function of the deposition method; electrodeposition and chemical deposition. Electrodeposition was performed at −2.0 V for 3 h. Figure 6 shows that in Hanks' solution, at the temperature of 37 ^oC, electrode coated with the electrodeposited Hap film has a higher polarization resistance (better barrier properties) compared to the electrode with hydroxyapatite film deposited by AIM. The protecting efficiency of the deposited HAp film was calculated using the relation:

$$\eta = (R_{p,(AZ91D)} - R_{p,(AZ91D|HAp)}) / R_{p,(AZ91D)} \quad (11)$$

R_p,(AZ91D|HAp) and R_p,(AZ91D) being the polarization resistance values of alloy specimens coated with HAp and those with a native surface layer, respectively. Data show that the η value of coating electrodeposited at −2.0 V for 3 h is about 10 % greater than those deposited by an alternative immersion method (AIM).

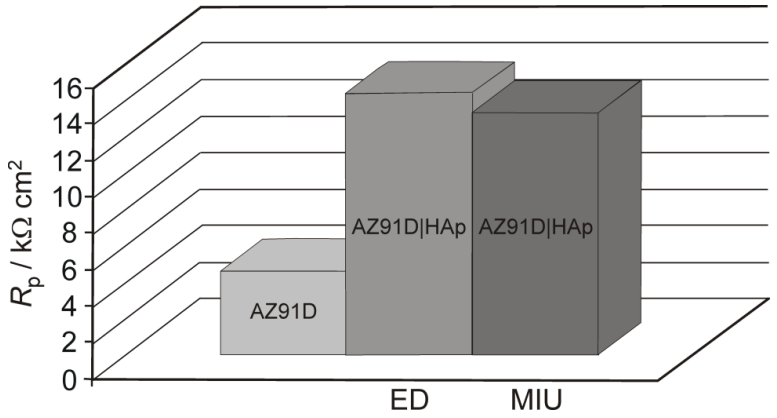

Figure 6. The values of R_p as a function of the deposition method; electrodeposition and chemical deposition. Electrodeposition was performed at −2.0 V for 3 h and chemical deposition by AIM.

4. CONCLUSION

In order to increase the bioactivity and biocompatibility the AZ91D alloy surface is modified with hydroxyapatite film by electrodeposition method and alternative immersion method (AIM).

On the AZ91D alloy surface electrodeposited brushite film and film of a β - TCP were converted into hydroxyapatite (Hap) via an acid-base reaction. AZ91D alloy modified with hydroxyapatite has a higher corrosion resistance in Hanks' solution in comparison to the unmodified AZ91D alloy. The protecting efficiency of HAp increases with the increasing deposition time to obtain a thicker and a more compact coating.

Electrodeposition method caused the formation of the surface film that provides higher polarization resistance values in comparison to the surface film formed by the alternative immersion method (AIM).

Chemical groups characteristic for HAp coating detected by FTIR spectroscopy on the coated AZ91D alloy confirmed the presence of the thick uniform layer of hydroxyapatite. Hydroxyapatite coated AZ91D alloy has good potential for use in medicine, because the HAp films has a good bioresorption.

ACKNOWLEDGEMENTS
The financial support of the Ministry of Science, Education and Sports of the Republic of Croatia under the 125-0982904-2932 is greatly appreciated.

List of symbols

B	time constant ($s^{1/2}$)
C	capacitance (F cm^{-2})
C_{dl}	electric double layer capacitance (F cm^{-2})
CPE	constant phase element
E	potential (V)
E_{corr}	corrosion potential (V)
E_{OCP}	open circuit potential (V)
f	frequency (Hz)
j	current density (A m^{-2})
j_{corr}	corrosion current density (A m^{-2})
$j\omega$	complex variable for sinusoidal perturbations with $\omega = 2f\pi$
l_p	pore length (m)
n	exponent of the constant phase element
N	number of pores
Q	constant of the constant phase element
r	pore radius (m)
R	resistance (Ω cm^2)
R_d	diffusion resistance (Ω cm^2)
R_{el}	ohmic resistance (Ω cm^2)
R_p	polarization resistance (Ω cm^2)
W_{S-P}	exponent of the Warburg element
W_{S-R}	resistance of the Warburg element (Ω cm^2)
W_{S-T}	time constant of the Warburg element (s)
Y_o	"addmitance" parameter (Ω^{-1} $s^{0.5}$ m^{-2})
Y_O	coefficient of the constant phase element (Ω^{-1} cm^{-2} s^n)
Z	electrode impedance (Ω cm^2)
Z_{imag}	imaginary part of the impedance (Ω cm^2)
Z_{real}	real part of the impedance (Ω cm^2)
Z_W	Warburg impedance (Ω cm^2)
$\|Z\|$	impedance modulus (Ω cm^2)

Greeks letters

θ	coverage
θ	phase angle (°)
v	wavenumber (cm^{-1})

α penetrability coefficient
η protecting efficiency
κ electrolyte conductivity (Ω^{-1} m^{-1})
λ penetration depth (m)
υ scan rate (mV s^{-1})
ω angular frequency (Hz)

References

1. Y. Xin, K. Huo, H. Tao, G. Tang and P. K. Chu, *Acta Biomater.*, 4 (2008) 2008
2. W. F. Ng, M. H. Wong and F. T. Cheng, *Surf. Coat. Techn.*, 204 (2010) 1823
3. H. Wong, K. W. K. Yeung, K. Lam, V. Tam, P. K. Chu, K. D. K. Luk and K. M. C. Cheung, *Biomaterials*, 31 (2010) 2084
4. G. Song, *Corros. Sci.*, 49 (2007) 1696
5. W. S. Pietrzak, *Tissue Eng.*, 6 (2000) 425
6. M. P. Staiger, A. M. Pietak, J. Huadmai and G. Dias, *Biomaterials*, 27 (2006) 1728
7. C. K. Seal, K. Vince and M. A. Hodgson, *Mater. Sci. Eng.*, 4 (2009) 012011
8. C. Choong, J-P. Griffiths, M. G. Moloney, J. Triffitt and D. Swallow, *React. Funct. Polym.*, 69 (2009) 77
9. W.-D. Mueller, M. L. Nascimento and M. Fernández Lorenzo de Mele, *Acta Biomater.* 6 (2010) 1749
10. Y. Xin, T. Hu, P. K. Chu, *Acta Biomater.*, 7 (2011) 1452
11. S. Zhang, X. Zhang, C. Zhao, J. Li, Y. Song, C. Xie, H. Tao, Y. Zhang, Y. He, Y. Jiang and Y. Bian, *Acta Biomater.*, 6 (2010) 626
12. F. Witte, V. Kaese, H. Haferkamp, E. Switzer, A. Meyer-Lindenberg, C. J. Wirth and H. Windhagen, *Biomaterials*, 26 (2005) 3557
13. H. X. Wang, S. K. Guan, X. Wang, C. X. Ren and L. G. Wang, *Acta Biomater.*, 6 (2010) 1743
14. Y. Xin, T. Hu and P. K. Chu, *J. Electrochem. Soc.* 157 (2010) C238
15. F. Witte, N. Hort, C. Vogt, S. Cohen, K. U. Kainer, R. Willumeit and F. Feyerabend, *Curr. Opin. Solid State Mater. Sci.*, 12 (2008) 63
16. E. D. McBride, *J. Am. Med. Assoc.*, 111 (1938) 2464
17. C. P. McCord, *Ind. Med.*, 11 (1942) 71
18. S. Hiromoto, A. Yamamoto, N. Maruyama, H. Somekawa and T. Mukai, *Corros. Sci.*, 50 (2008) 3561
19. K. Brunelli, M. Dabalà, I. Calliari and M. Magrini, *Corros. Sci.*, 47 (2005) 989
20. Y. Tamar and D. Mandler, *Electrochim. Acta*, 53 (2008) 5118
21. Y. Liu, Z. Yu, S. Zhou and L. Wu, *Appl. Surf. Sci.*, 252 (2006) 3818
22. M. F. Montemora and M. G. S. Ferreira, *Electrochim. Acta*, 52 (2007) 7486
23. C. Wen, S. Guan, L. Peng, C. Ren, X. Wang and Z. Hu, *Appl. Surf. Sci.*, 255 (2009) 6433
24. F. Geng, L. L. Tan, X. X. Jin, J.Y. Yang and K. Yang, *J. Mater. Sci.: Mater. Med.*, 20 (2009) 1149
25. Y. Zhang, G. Zhang and M. Wei, *J. Biomed. Mater. Res. B*, 89 B (2009) 408
26. J-H. Jo, B-G. Kang, K-S. Shin, H-E. Kim, B-D. Hahn, D-S. Park and Y-H. Koh, *J. Mater. Sci.: Mater. Med.*, 22 (2011) 2437
27. Y. W. Song, D. Y. Shan and E. H. Han, *Mater. Lett.*, 62 (2008) 3276
28. R. Narayanan and S. K. Seshadri, *Mater. Chem. Phys.*, 106 (2007) 406
29. M. C. Kuo and S. K. Yen, *Mater. Sci. Eng. C*, 20 (2002) 153
30. B. A. Boukamp, *Solid State Ionics*, 20 (1986) 31

31. M. Metikoš-Huković, R. Babić, Z. Grubač, M. Petravić and P. Robert, *J. Electrochem. Soc.*, 160 (2013) H674
32. Y. Song, S. Zhang, J. Li, C. Zhao and X. Zhang, *Acta Biomater.*, 6 (2010) 1736
33. M. B. Kannan and L. Orr, Biomed. Mater. 6 (2011) 045003
34. M. Kumar, H. Dasarathy and C. Riley, *J. Biomed. Mater. Res. Part A*, 45 (1999) 302
35. S. Shadanbaz and G. J. Dias, *Acta Biomater.*, 8 (2012) 20
36. J. R. Macdonald, Impedance Spectroscopy: Emphasizing Solid Materials and Systems, John Wiley & Sons, New York (1987)
37. J. Lukacs, *J. Electroanal. Chem*., 464 (1999) 68
38. J. R Macdonald, *J. Electroanal. Chem*., 378 (1994) 17
39. H-K. Song, Y-H. Jung, K-Hg Lee and L. H. Dao, *Electrochim. Acta*, 44 (1999) 3513
40. H-K. Song, H-Y. Hwang, K-H. Lee and L. H. Dao, *Electrochim. Acta*, 45 (2000) 2241
41. R. de Levie, *Advances in Electrochemistry and Electrochemical Engineering*, Interscience, New York (1967)
42. K. Eloot, F. Debuyck, M. Moors and A. P. Van Peteghem, *J. Appl. Electrochem.*, 25 (1995) 334
43. D. D. Macdonald, M. Urquidi-Macdonald, S. D. Bhakta and B. G. Pound, *J. Electrochem Soc.*, 138 (1991) 1359
44. L. Valek, M. Metikoš-Huković and Z. Grubač, *J. New. Mat. Electrochem. Syst.*, 9 (2006) 145
45. Z. Grubač, M. Metikoš-Huković and R. Babić, *Electrochim. Acta*, 109 (2013) 694
46. M. Tomozawa, S. Hiromoto and Y. Harada, *Surf. Coat. Tech.*, 204 (2010) 3243
47. L. Birry and A. Lasia, *J. Appl. Electrochem.*, 34 (2004) 735
48. B. Losiewicz, A. Budniok, E. Rowinski, E. Lagiewka and A. Lasia, *J. Appl. Electrochem.*, 34 (2004) 507
49. A. Lasia, *„Application of the Electrochemical Impedance Spectroscopy to Hydrogen Adsorption, Evolution and Absorption into Metals", Modern Aspects of Electrochemistry*, Plenum Press, New York, (2002)
50. M. B. Kannan and R. K. S. Raman, *Biomaterials*, 29 (2008) 2306
51. Z. Grubač, I. Škugor-Rončević, M. Metikoš-Huković, R. Babić, M. Petravić and R. Peter, *J. Eelectrochem. Soc.*, 159 (2012) C1
52. Z. Grubač, M. Metikoš-Huković, R. Babić, I. Škugor Rončević, M. Petravić and R. Peter, *Mater. Sci. Eng. C*, 33 (2013) 2152
53. G. Song, A. Atrens and M. Dargusch, *Corros. Sci.*, 41 (1999) 249
54. M. Tomozawa and S. Hiromoto, *Appl. Surf. Sci.*, 257 (2011) 8253
55. M. B. Kannan and O. Wallipa, *Mater. Sci. Eng. C*, 33 (2013) 675
56. C. M. Turhan and S. Virtanen, *Surface modification of Mg and Mg alloys, in: Exploring new aspects*, Academic Press, Saarbrűcken, (2012)
57. Y.-H. Li and S. Gregory, *Geochim. Cosmochim. Acta*, 88 (1974) 703
58. B. Chen and C. Liang, *Ceram. Int.*, 33 (2007) 701
59. N. Pleshko, A. Boskey and R. Mendelsohn, *Biophys J.*, 60 (1991) 786
60. J. E. Gray-Munro and M. Strong, *J. Biomed. Mater. Res., Part A*, (2008) 339
61. S. V. Dorozhkin, *Prog. Cryst. Growth Charact. Mater.*, 44 (2002) 45
62. M. Ashok, N. M. Sunderam and S. N. Kalkura, *Mater. Lett.*, 57 (2003) 2066
63. R. M. Trommer, L. A. Santos and C. P. Bergman, *Mater. Sci. Eng., C*, 29 (2009) 1770
64. L. Müller and F. A. Müller, *Acta Biomater.*, 2 (2006) 181
65. J. Katić, M. Metikoš-Huković and R. Babić, *J. Appl. Electrochem.*, 44 (2014) 87
66. L. Mohan, D. Durgalakshmi, M. Geetha, T. S. N. Sankara Narayanan and R. Asokamani, *Ceram. Int.*, 38 (2012) 3435
67. J. Katić, M. Metikoš-Huković, R. Babić and M. Marciuš, *Int. J. Electrochem. Sci.*, 8 (2013) 1394
68. A. Stoch, W. Jastrzębski, A. Brożek, J. Stock, J. Szarinec, B. Trybalska and G. Kmita, *J. Mol. Struct.*, 555 (2000) 375

69. T. A. Kuriakose, S. N. Kalkura, M. Palanichamy, D. Arivuoli, K. Dierks, G. Bocelli and C. Betzel, *J. Cryst. Growth*, 263 (2004) 517
70. T. Hayakawa, M. Kawashita and G. H. Takaoaka, *J. Ceram. Soc. Jpn.*, 116 (2008) 68
71. A. Kodama, S. Bauer, A. Komatsu, H. Asoh, S. Ono and P. Schmuki, *Acta Biomater.*, 5 (2009) 2322